Running into trouble with the time-dependent propagation of a wavepacket

2010 Eur. J. Phys. 31 785

(http://iopscience.iop.org/0143-0807/31/4/008)

IOP PUBLISHING EUROPEAN JOURNAL OF PHYSICS

Eur. J. Phys. **31** (2010) 785–799 doi:10.1088/0143-0807/31/4/008

Running into trouble with the time-dependent propagation of a wavepacket

Abel E Garriz[1], Alejandro Sztrajman[1,2] and Darío Mitnik[1,2]

[1] Instituto de Astronomía y Física del Espacio, C.C. 67, Suc. 28, (C1428EGA) Buenos Aires, Argentina
[2] Departamento de Física, Facultad de Ciencias Exactas y Naturales, Universidad de Buenos Aires, Argentina

E-mail: dmitnik@df.uba.ar

Received 26 January 2010, in final form 16 April 2010
Published 26 May 2010
Online at stacks.iop.org/EJP/31/785

Abstract

The propagation in time of a wavepacket is a conceptually rich problem suitable to be studied in any introductory quantum mechanics course. This subject is covered analytically in most of the standard textbooks. Computer simulations have become a widespread pedagogical tool, easily implemented in computer labs and in classroom demonstrations. However, we have detected issues raising difficulties in the practical effectuation of these codes which are especially evident when discrete grid methods are used. One issue—relatively well known—appears at high incident energies, producing a wavepacket slower than expected theoretically. The other issue, which appears at low wavepacket energies, does not affect the time evolution of the propagating wavepacket proper, but produces dramatic effects on its spectral decomposition. The origin of the troubles is investigated, and different ways to deal with these issues are proposed. Finally, we show how this problem is manifested and solved in the practical case of the electronic spectra of a metal surface ionized by an ultrashort laser pulse.

(Some figures in this article are in colour only in the electronic version)

1. Introduction

The propagation of a one-dimensional wavepacket by the time-dependent Schrödinger equation has become a standard pedagogical tool for any undergraduate quantum physics course. It allows the visualization of many of the elementary concepts of quantum mechanics. In the first place, it is a vivid representation of the way in which the Schrödinger equation plays a role logically analogous to Newton's second law: given suitable initial conditions for the wavefunction, they determine the wavefunction for all future time [1]. Many fundamental

concepts of quantum theory, such as wave–particle duality, the uncertainty principle and the meaning of the wavefunction, can easily be illustrated by using a wavepacket example. The conceptual richness of its time propagation helps to understand basic but not straightforward concepts like the meaning of the representation of a particle as a combination of waves, the differences between phase and group velocities, and the spreading of a wavepacket, among many others. Moreover, the application of simple visualization techniques allows one to depict in a very comprehensible way phenomena such as tunnelling, resonances, coherent and squeezed states, rebounding and revivals. In such cases, the notions gained by watching a movie can hardly be obtained by other means.

Remarkably, the time evolution of a wavepacket can be implemented with simple computer simulations; it does not require any sophisticated programming techniques or costly computational resources. A wide bibliography with all the details required for the calculations is available [2–8]. In general, by choosing adequate parameters for the time-step evolution, most of the codes can be robust, even if one includes potential barriers or wells to show the transmission, reflection and resonance phenomena.

Therefore, this subject is an excellent candidate for producing an 'on the fly' demonstration in the classroom. However, there are some important issues that one should be aware of in order to avoid odd results. The first issue may appear when one is interested in the calculation of the velocity of the propagated wavepacket. In general, a wavepacket slower than theoretically expected may be found. The higher the energy of the incident wavepacket, the more evident the retardation effect. This problem is relatively well known, and has both a simple explanation and solution, as discussed in section 2. We present here another issue, which appears mainly at low incident energies. It does not affect the time evolution of the propagated wavepacket proper, but produces dramatic consequences in its spectral decomposition. When looking at the coefficients of the expansion of the wavepacket on a stationary eigenfunction basis, the resulting spectrum may be far different from expected, and will in general be contaminated by spurious and huge oscillations. Finally, in section 4, we show how this problem is manifested and solved in the practical case of the electronic spectra of a metal surface ionized by an ultrashort laser pulse.

Atomic units are used throughout this work, so the velocity v, the momentum $p = mv$ and the wave number $k = p/\hbar$ are numerically indistinguishable.

2. Problems in the propagation of high-energy wavepackets

In this section, we will analyse the simplest quantum-mechanical scattering case, which is a localized one-dimensional wavepacket moving towards a region where a potential exists. The wavepacket is initially centred at some position x_0 with a spatial spread σ_x and having an average wave number k_0, which is also (in the units used) the initial velocity of the packet. This analysis requires the solution of the time-dependent Schrödinger equation

$$\begin{aligned} \mathrm{i}\frac{\partial \Psi(x,t)}{\partial t} &= \hat{H}\Psi(x,t) \\ &= -\frac{1}{2}\frac{\partial^2 \Psi(x,t)}{\partial^2 x} + V(x,t)\Psi(x,t), \end{aligned} \tag{1}$$

which determines completely the time evolution of the initial wavepacket.

The more instructive way to solve the Schrödinger equation (suitable for a quantum mechanics course) is via a finite difference method that transforms the differential problem into an algebraic problem. First, the wavefunction is discretized in a numerical grid, and the

spatial interval $[x_{\min}, x_{\max}]$ is divided into equidistant points with a mesh size Δx, resulting in the grid

$$x_{\min} = x_1, x_2, \ldots, x_N = x_{\max}. \tag{2}$$

The time is also discretized, so the various t values become $t_n = n\Delta t$. We denote by

$$\phi_j^i = \Psi(x_j, t_i) \tag{3}$$

the value of the discretized wavefunction at point x_j and time t_i. In this discrete notation, the first-order approximation of the Hamiltonian in equation (1) becomes

$$\hat{H}\phi_j^i = \frac{-\phi_{j+1}^i + 2\phi_j^i - \phi_{j-1}^i}{2\Delta x^2} + V_j^i \phi_j^i, \tag{4}$$

where $V_j^i = V(x_j, t_i)$. Using this approximation, the Hamiltonian is represented by a tri-diagonal matrix, usually known as a three-point spatial stencil.

Many simple computer algorithms can be used for the study of a wavepacket propagated in time. The problem we are analysing does not relate to the particular scheme used for the time propagation, regardless of whether they are explicit or implicit algorithms. It appears in any numerical calculation, ranging from the simplest Euler propagation scheme to Crank–Nicolson, split-operators or leap-frog methods. It even appears if a time-independent potential is assumed. Therefore, for the sake of simplicity, we will illustrate the different features in the simplest case, a wavepacket propagated in a zero potential ($V(x, t) = 0$).

If the evolution occurs in a potential-free region, the group velocity should be the same at any time. A good test for the numerical method used in the propagation is to watch the position of the wavepacket at different times. That should give the group velocity of the packet, which must correspond to its incident energy. However, we present here an issue that appears at high incident energies where, in general, a wavepacket slower than theoretically expected is obtained. The higher the energy of the wavepacket, the more evident the retardation effect. As an example, we consider the following incident Gaussian wavepacket:

$$\Psi(x, t = 0) = \frac{1}{\sqrt{\sqrt{\pi}\sigma_x}} \mathrm{e}^{-\frac{1}{2}(\frac{x-x_0}{\sigma_x})^2 + \mathrm{i}k_0 x} \tag{5}$$

where the wavepacket width $\sigma_x = 1$ au, its initial position $x_0 = 10$ au and the initial velocity $k_0 = 10$ au. In the following calculations, a numerical grid of $N = 500$ points with a spatial discretization of $\Delta x = 0.06$ au is used.

The numerical probability density $|\Psi|^2$ of the propagated wavepacket is plotted in figure 1(a), at successive times $t = 0, 0.15, 0.3, 0.45, 0.6$ and 0.75 au. For each time, the analytical results are also plotted for comparison, showing a slight retardation of the numerically propagated waves.

As shown in the analytic results, the centre of the wavepacket should be located, at $t = 0.75$ au, at a position $x = 17.5$ au. However, the curve showing the numerical result at this time has its maximum at $x \approx 17.05$ au. The probability density of the Fourier transform of the propagated wavepacket (which results in the same picture at any time) is shown in figure 1(b). As expected, the transformed wave is another Gaussian, centred at $k_0 = 10$ au and having a width $\sigma_k = \frac{1}{\sigma_x} = 1$ au.

A more dramatic case is shown in figure 2(a) where the initial wavepacket velocity is $k_0 = 45$ au. The figure shows that at time $t = 0.75$ au, the centre of the wavepacket is displaced about 5.3 au from the origin, which means a velocity of $v \approx 7.15$ au, roughly six times smaller than the theoretical value. The Fourier transformed wavepacket is shown in part (b) of the figure, but again, it does not give any clue regarding the origin of the discrepancies in the velocities.

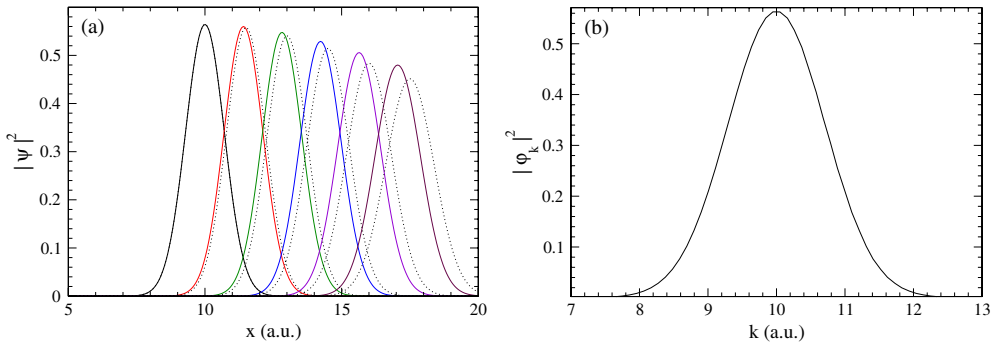

Figure 1. (a) Propagation of a free wavepacket having an initial position $x_0 = 10$ au, a spatial width $\sigma_x = 1$ au and an initial velocity $k_0 = 10$ au. The numerical method employed used a first-order approximation for the spatial derivatives, with a grid size of $\Delta x = 0.06$ au. Solid curves: numerical propagation at times $t = 0, 0.15, 0.3, 0.45, 0.6$ and 0.75 au. Dotted lines: analytical results. (b) Momentum distribution of the same wavepacket.

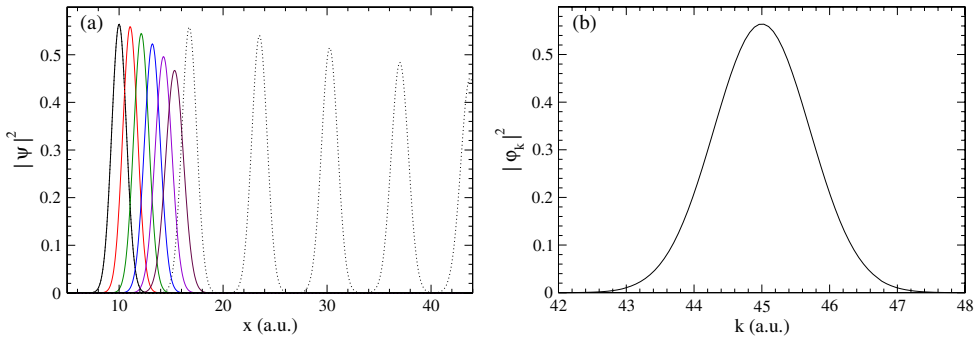

Figure 2. (a) Propagation of a free wavepacket having an initial position $x_0 = 10$ au, a spatial width $\sigma_x = 1$ au and an initial velocity $k_0 = 45$ au. The numerical method employed used a first-order approximation for the spatial derivatives, with a grid size of $\Delta x = 0.06$ au. Solid curves: numerical propagation at times $t = 0, 0.15, 0.3, 0.45, 0.6$ and 0.75 au. Dotted lines: analytical results. (b) Momentum distribution of the same wavepacket.

In order to summarize the different results, we have calculated (using a three-point spatial stencil) the numerical velocities v_{num} (given by the ratio between the position of the centre of the wavepacket and the time), and compared them with the incident wavepacket velocities v. These results are shown in figure 3, where the retardation of the numerical wavepackets becomes clear.

The curve v_{num} versus v is sinusoidal, instead of being a straight line. That means that only for low velocities does the numerical propagation produce reasonable results. We found that the numerical propagated wavepacket reaches the maximal velocity at an incident velocity $v_{\text{num}} = 26.17$ au. Moreover, for a wavepacket having a theoretical initial velocity of $v = 52.36$ au, its numerical propagation will result in a standing wave. Even worse, for higher initial velocities, the wavepacket will propagate in the opposite direction!

The origin of the problems is related to the discretization of the space coordinate, which is mandatory in any numerical grid method. This imposes the impossibility of representing a wave having a wavelength smaller than the discretization size of the numerical grid. In an

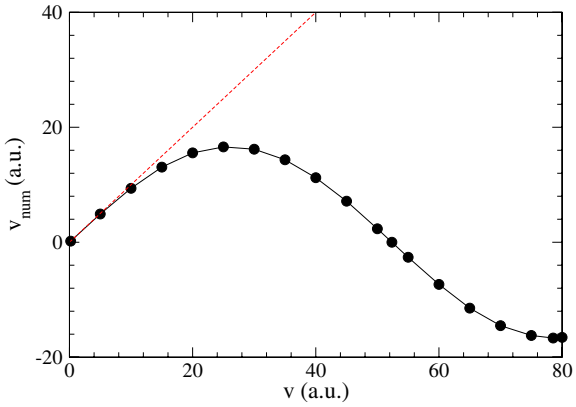

Figure 3. Numerical velocities v_{num} of the propagated wavepacket (first-order approximation for derivatives and $\Delta x = 0.06$ au), compared with the theoretical results v.

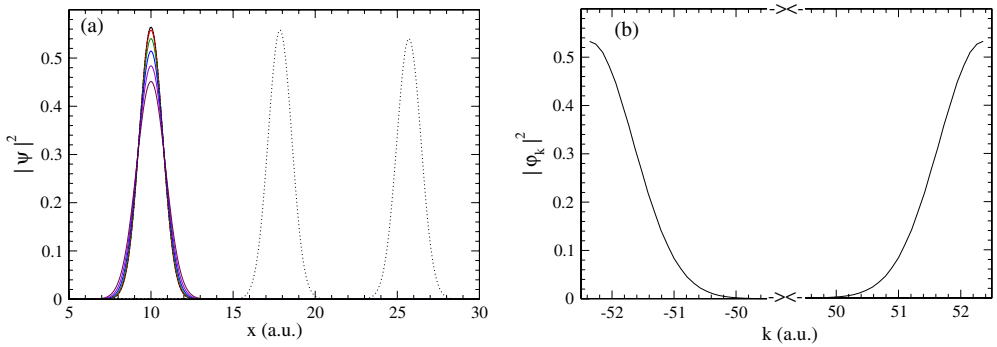

Figure 4. (a) Propagation of a free wavepacket, having an initial position $x_0 = 10$ au, a spatial width $\sigma_x = 1$ au and an initial velocity $k_0 = 52.36$ au. The numerical method employed used a first-order approximation for the spatial derivatives, with a grid size of $\Delta x = 0.06$ au. Solid curves: numerical propagation at times $t = 0, 0.15, 0.3, 0.45, 0.6$ and 0.75 au. Dotted lines: analytical results (only for $t = 0, 0.15$ and 0.3 au). (b) Momentum distribution of the same wavepacket.

infinite square well potential of width L, the wave number $k_n = \frac{\pi}{L}n$. Thus, the maximum momentum that can be described with a numerical grid having a mesh size Δx is given by[3]

$$k_{\mathrm{max}} = \frac{\pi}{L}n_{\mathrm{max}} = \frac{\pi}{\Delta x}. \tag{6}$$

If the initial wavepacket contains wave components having a momentum similar to or larger than this limit, the results of the evolution will not match that obtained from the analytical solution of the Schrödinger equation.

In our numerical calculations (with $\Delta x = 0.06$ au), the maximum momentum allowed by equation (6) is $k_{\mathrm{max}} = 52.36$ au. The time evolution of a wavepacket having that incident velocity value is shown in figure 4(a), where the numerical wavepacket is indeed a wave with zero velocity.

[3] We want to note that in our numerical results using a first-order approximation for the spatial derivatives, the wavenumber of the highest energy level obtained in the diagonalization of the Hamiltonian tends to $k_h = \frac{2}{\Delta x}$, rather than the k_{max} value expressed in equation (6).

The numerical Fourier transform of a given function can be quite different from the mathematical one. That is well illustrated in figure 4(b), where the aliasing effect occurs as a consequence of trying to represent frequencies higher than the Nyquist frequency (the highest frequency that can be coded at a given sampling rate in order to be able to fully reconstruct the signal [9]). Any component of the wavepacket having a wavenumber k_i outside the $(-\pi/\Delta x, \pi/\Delta x)$ interval is treated as $k_i = k_i' + 2\pi n/\Delta x$, with n being an integer such that $k_i' \in (-\pi/\Delta x, \pi/\Delta x)$. That produces a chopping in the high-energy components of the wavepacket, reducing the global group velocity.

The Fourier transformed wavepacket should be well represented in the numerical grid. Denoting as k_m the largest momentum present to any appreciable extent in the wavepacket, e.g.

$$k_m \approx k_0 + 2\sigma_k, \tag{7}$$

it is obviously mandatory that

$$k_m < k_{\max} \tag{8}$$

which is equivalent to imposing a limitation in the wavepacket velocity

$$v < \frac{\pi}{\Delta x} - \frac{2}{\sigma_x}. \tag{9}$$

That condition is largely fulfilled in the cases presented in figures 1 and 2, that, however, show a considerable retardation of the wavepacket evolution. The discretization scheme used in the calculations requires additional conditions to be satisfied in order to avoid this problem.

Considering the free wavepacket propagation with no potential at all, the solution of the Schrödinger equation for the k wave

$$\hat{H}\phi_k = -\frac{1}{2}\frac{\partial^2}{\partial x^2}\phi_k(x) = \frac{k^2}{2}\phi_k(x) \tag{10}$$

is a plane wave

$$\phi_k(x) = \sin kx. \tag{11}$$

Using a first-order approximation for the spatial derivatives and denoting the discretized wave $\phi_k^j = \phi_k(x_j) = \sin kx_j$,

$$\frac{\partial^2}{\partial x^2}\phi_k(x_j) \approx \frac{\phi_k^{j+1} - 2\phi_k^j + \phi_k^{j-1}}{\Delta x^2} = \frac{2\sin kx_j(\cos k\Delta x - 1)}{\Delta x^2}. \tag{12}$$

For a small $k\Delta x$ this may be approximated by

$$\frac{\partial^2}{\partial x^2}\phi^k(x_j) \approx k^2\left(\frac{(k\Delta x)^2}{12} - 1\right)\sin kx_j. \tag{13}$$

In order that equation (4) be an accurate approximation for every wavepacket component, even for the largest k_m, i.e.

$$-k_m^2 \sin k_m x_j \approx k_m^2\left(\frac{(k_m\Delta x)^2}{12} - 1\right)\sin k_m x_j, \tag{14}$$

the condition

$$\Delta x \ll \frac{\sqrt{12}}{k_m} \tag{15}$$

must be satisfied.

Understanding the origin of this problem allows for its simple solution, i.e. to reduce the numerical grid discretization size. However, there is another way to solve this problem, and

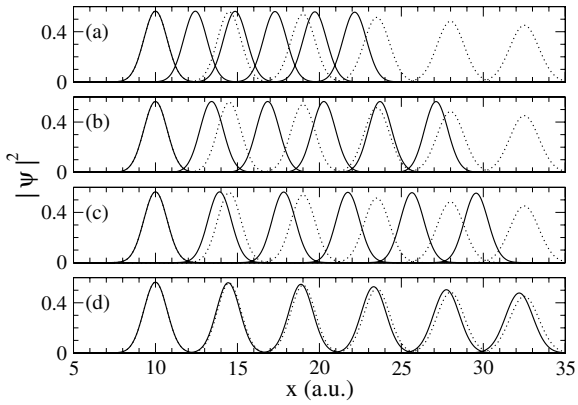

Figure 5. Propagation of a free wavepacket, having an initial position $x_0 = 10$ au, a spatial width $\sigma_x = 1$ au and an initial velocity $k_0 = 30$ au. The numerical method employed used a grid size of $\Delta x = 0.06$ au. Solid curves: numerical propagation at times $t = 0, 0.15, 0.3, 0.45, 0.6$ and 0.75 au. Dotted lines: analytical results. (a) First-order approximation for the second-order spatial derivative (tri-diagonal matrix). (b) Five-point approximation for the second-order spatial derivative (penta-diagonal matrix). (c) Seven-point approximation for the second-order spatial derivative. (c) 15-point approximation for the second-order spatial derivative.

it consists of improving the spatial scheme for the finite-difference approximation. Replacing the tri-diagonal matrix used in the representation of the Hamiltonian by a penta-diagonal or a higher order approximation for the second-order derivatives improves dramatically the achievable precision without adding any important amount of computational time (see, for example, [10] and [11] with references within). For our concerns, these improved space-discretization schemes have another beneficial effect. The three-point approximation for the second-order spatial derivatives cannot resolve the Fourier components that do not fulfil the condition given in equation (15). However, a higher order scheme will allow us to resolve higher frequency components. Thus, these schemes displace the high-energy component cutoffs to higher energies. As an example, in figure 5 we show the propagation of the same free wavepacket of the previous figures, but now the initial velocity is $k_0 = 30$ au. A numerical method using a first-order (three-point) approximation for the second-order spatial derivative (as shown in figure 3) produces a propagated wavefunction with a velocity $v_{\mathrm{num}} = 16.2$ au. The propagated wavepacket at different times is shown in part (a) of figure 5, together with the analytical results. Improving the spatial derivatives scheme will reduce the delay of the time propagation, although we are still using the same numerical grid. For example, in part (b) of the same figure the results of a numerical propagation which uses a five-point matrix representation are shown. In this case, the velocity $v_{\mathrm{num}} = 22.7$ au is much closer to the expected value of $v = 30$ au. We can improve the calculations even more, as shown in part (c) of the figure, where a seven-point approximation propagates the wavepacket with $v_{\mathrm{num}} = 26.1$ au. In part (d) of the same figure, a 15-point approximation is used, producing a wavepacket propagated with $v_{\mathrm{num}} = 29.6$ au.

3. Problems in the propagation of low-energy wavepackets

A different kind of problem appears in the propagation of low-velocity wavepackets. These problems are more elusive, since they do not occur in the propagation itself, but in the spectral projection. Let us first discuss the case in which the potential V in equation (1) is independent

of the time t. In that case the Schrödinger equation is separable and the solution can be written as

$$\Phi(x,t) = \varphi(x)\, f(t). \tag{16}$$

The separation of variables leads to convert the time-dependent Schrödinger equation into two ordinary differential equations [1]. The solution of the equation dependent on time is

$$f(t) = \mathrm{e}^{-\mathrm{i}Et} \tag{17}$$

where the energy E is the separation constant. The spatial equation is the time-independent Schrödinger equation

$$\hat{H}(x)\varphi(x) \equiv -\frac{1}{2}\frac{\mathrm{d}^2\varphi(x)}{\mathrm{d}x^2} + V(x)\varphi(x) = E\varphi(x). \tag{18}$$

In order to distinguish the various possible values of the energy E (and their corresponding eigenfunctions $\varphi(x)$), we label them with an index k. Thus, we have

$$\hat{H}(x)\varphi_k(x) = E_k\varphi_k(x). \tag{19}$$

For simplicity, we assume a Hermitian, non-degenerate Hamiltonian H with a discrete spectrum. Then, any spatial wavefunction $\psi(x)$ can be written as a linear combination of the energy eigenstate basis functions, i.e.

$$\psi(x) = \sum_k c_k\, \varphi_k(x), \tag{20}$$

where

$$c_k = \langle \psi(x) | \varphi_k(x) \rangle. \tag{21}$$

If the Hamiltonian is not an explicit function of time, this expansion is also useful to provide the evolution in time of any quantum state. Denoting

$$\Psi(x, t=0) \equiv \psi(x), \tag{22}$$

then, this initial state evolves in time as [12, 13]:

$$\Psi(x,t) = \sum_k c_k\, \mathrm{e}^{-\mathrm{i}E_k t}\varphi_k(x). \tag{23}$$

The procedure can easily be generalized to the case where the spectrum of H is continuous. In that case, the expansion becomes, with obvious notation,

$$\Psi(x,t) = \int c_E\, \mathrm{e}^{-\mathrm{i}Et}\varphi_E(x)\, \mathrm{d}E. \tag{24}$$

Expansion (23) is a fundamental concept of quantum theory, and provides a very simple way to perform the time evolution of a quantum system. Pedagogically, this expansion helps to understand many concepts related to the dynamics of a quantum system—from the spreading of a wavepacket to coherent states—and many elementary examples can easily be provided (see, for instance, simple Mathematica examples in [14]). The projection coefficients c_k are very useful for many reasons. If the Hamiltonian does not depend on time, checking the invariance of the expansion coefficients at different steps of the temporal evolution should provide a good quality test of the numerical methods employed and the eigenfunctions used. For potentials depending on time like those used in collision processes, these coefficients are fully related to the probability yield of the different inelastic channels. In the last part of this work we show the electronic spectra of a metal surface ionized by an ultrashort laser pulse. These spectra are obtained by plotting the coefficients c_k as a function of the emitted electron energy.

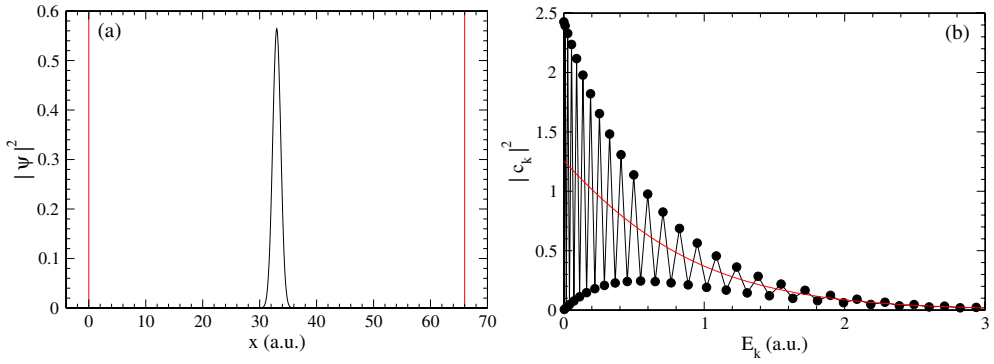

Figure 6. (a) Initial wavepacket equation (5), for $k_0 = 0.5$ au, centred at $x_0 = 33$ au. The box containing the numerical grid is also shown in the figure. (b) Numerical spectral decomposition (equation (21)) of this initial wavepacket. Smooth curve: proper results.

The Schrödinger equation is a partial differential equation, normally defined on an unbounded domain with definite boundary conditions (for bound states, they tend to zero towards the end of the domain). In order to make the calculations feasible for numerical treatment it is necessary, in general, to restrict the original problem to a finite interval. Moreover, the energy eigenvector basis set can be infinite dimensional; therefore, a truncation of expansions like (23) is mandatory for any practical numerical calculation. A simple and pedagogical way to conform both restrictions is by using a finite difference method representing the Hamiltonian by a matrix, as shown in equation (4) and explained in section 2. Thus, the simplest recipe to propagate a general initial state in time would be as follows: for a given potential, the Hamiltonian matrix is constructed, by discretizing the spatial coordinate. Using standard diagonalization techniques, the eigenvalues E_k and eigenvectors $\varphi_k(x)$ are obtained. Then, the initial wavefunction $\psi(x)$ is projected as shown in equation (21), obtaining the projection coefficients c_k. Finally, the function at any time is calculated via the time evolution (equation (23)).

However, this procedure may produce results quite different from what was expected, when one analyses the projection coefficients of a wavefunction $\Psi(x, t)$ evolving in time from an initial wave $\psi(x) \equiv \Psi(x, t = 0)$. As an example, in figure 6(b) we show the value of different coefficients c_k as a function of the energy E_k, for the initial Gaussian wavepacket function $\psi(x)$ given in equation (5), having an incident velocity $k_0 = 0.5$ au and centred at the middle of the numerical grid, as shown in figure 6(a). In this case, we extended the numerical grid using 1100 points, so that it covers the range between $x = 0$ and $x_{\max} = 66$ au. Therefore, a wavepacket located in the centre of this numerical grid has $x_0 = 33$ au. (see figure 6(a)). The numerical grid also determines the energy eigenvalues. For this case, the spectrum consists of 1100 values spread between 1.13×10^{-3} au and 556 au. Within the range covered in the figure (between 0 and 3 au), the discretized Hamiltonian has 52 eigenvectors. The wavepacket reconstructed from the spectral decomposition (23) using the 1100 $\varphi_k(x)$ eigenvectors is completely undistinguishable from the initial Gaussian wavepacket; therefore, it is not displayed in figure 6(a). This spectral decomposition shows huge oscillations, while the expected spectrum is a smooth decreasing exponential function. Clear evidence that the oscillations in the projection spectra are a spurious effect is shown in figure 7(b), where the same spectrum is calculated, but now the initial wavepacket is shifted 10 au to the left ($x_0 = 23$ au, see figure 7(a)).

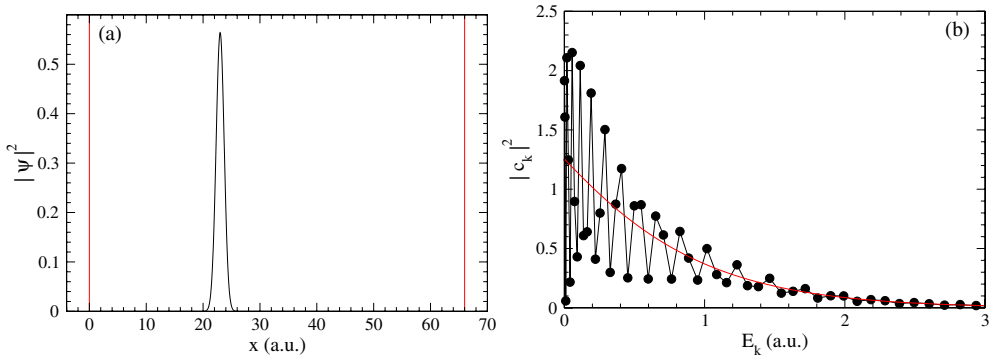

Figure 7. (a) Initial wavepacket equation (5), for $k_0 = 0.5$ au, centred at $x_0 = 23$ au. The box containing the numerical grid is also shown in the figure. (b) Numerical spectral decomposition (equation (21)) of this initial wavepacket. Smooth curve: proper results.

Obviously, the coefficients of the expansion, which reflect the amplitude of the different waves conforming the wavepacket, cannot depend on its position; therefore, these results are physically incorrect. The appropriate results (obtained by using a procedure described at the end of the section (see equation (27))) are shown in the same figures, with a smooth curve.

The origin of the oscillations resides primarily in the fact that the potential is symmetric around its centre, supplemented with the use of parity-defined stationary eigenvectors. It is known [15] that all the eigenfunctions of a symmetric potential are either even or odd with respect to reversions of the spatial coordinate around the symmetry axis. That is true even in the case of the free potential when it is discretized on a numerical grid. In space coordinates, a finite numerical matrix means that the operator as well as its eigenvectors is zero outside the range of the matrix. Therefore, what is actually solved using the finite difference method is not the Schrödinger equation for a desired potential, but for this same potential confined in a box. Since all the wavefunctions must be continuous, their values at the boundaries must also be zero. This leads (still for the free particle potential) to stationary eigenvectors having a definite parity, successively alternating between even and odd functions. The initial wavepacket centred at the middle of the numerical grid is not strictly an even function due to the presence of the velocity factor ik_0x in the exponent (see equation (5)). Nevertheless, it is very similar to an even function, especially for low incident energies. Since any projection between functions of opposite parity is zero, the numerical results oscillate around the right values, according to the parity of the Hamiltonian eigenvector basis. When the initial wavepacket is displaced from the centre of the box, as in figure 7, the spatial symmetry is not completely removed. The axis of symmetry of the initial wavefunction is shifted, and therefore, the projections are no longer products of functions with a definite parity. Even so, the oscillating pattern evidences that some kind of parity still remains in the wavepacket components. It is possible to shift the initial wavepacket even more, diminishing the oscillations, but it is impossible to fully eliminate them. As we mentioned before, the effect is elusive because it does not alter the propagation of the wavefunction. In fact, the functions reconstructed from the spectral decomposition (23) and the correspondent time-evolving wavefunctions will not be distinguishable at any time. Moreover, the unphysical oscillations in the projected spectra are not related to the particular numerical method used in the time propagation, since the

projected spectra shown in figures 6(b) and 7(b) have been calculated at the initial time, before the time evolution.

If this effect distorts the spectra of the incident wavepacket in such a striking way, it will, consequently, also alter dramatically the spectra of the evolving wave. For time-dependent processes, where the coefficients are related to probabilities of different processes, these oscillations can spoil the calculations, producing meaningless results.

There are many ways to avoid the problems presented in the present section. In all of them it is necessary to break the parity of the stationary states. As discussed above, it is not enough to make a shift in the spatial coordinates, because that would only change the oscillations, rather than eliminate them. A possible solution is to impose different values on the wavefunctions at the boundaries by controlling the extremal elements of the Hamiltonian matrix. Thus, the diagonalization procedure would lead to eigenfunctions without a defined parity. However, this procedure is equivalent, in its consequences, to a change in the size of the box. The diagonalization will only produce a different set of eigenvectors, with different energies, but the spectral projection would still have oscillations; they would just appear at different positions.

The failure of the change in the boundary conditions of the stationary eigenvectors as a solution of the oscillations problem suggests that what needs to be changed is the stationary condition of the eigenvectors itself. Matrix Hamiltonians with outgoing boundary conditions (also called transparent boundary conditions) can also be constructed by changes in the extremal elements of the matrix (see, for example, [16]). For a wavefunction discretized in a spatial interval $[x_0 = x_{\min}, x_N = x_{\max}]$ a transparent boundary condition can be imposed on the functions by assuming that the wavefunction has already reached the correct asymptotic behaviour, so

$$\frac{\varphi_{N+1}}{\varphi_N} = \frac{\varphi_N}{\varphi_{N-1}}. \tag{25}$$

For the wavepacket (5) having an initial velocity k_0, the transparent boundary condition becomes

$$\frac{\varphi_N}{\varphi_{N-1}} = \frac{\mathrm{e}^{\mathrm{i}\,k_0\,x_N}}{\mathrm{e}^{\mathrm{i}\,k_0\,x_{N-1}}} = \mathrm{e}^{\mathrm{i}\,k_0\,\Delta x}, \tag{26}$$

determining the modified value of φ_N. That new value at the boundary modifies the whole differential equation and its matrix representation, which is now complex. The diagonalization of this matrix may produce the desired eigenfunctions, suitable for the spectral projections.

A different way proposed here to solve the projection problem is to generate a continuum set of outgoing wavefunctions. For a general short-range potential we employ two sets of basis functions, φ_k^L and φ_k^R, having outgoing conditions (to the left and right, respectively), as depicted in figure 8. Numerical integration of the Schrödinger equation is employed to generate the functions, constrained to the imposed boundary conditions. These functions are complex, and in general, the dephasing among the real and imaginary parts mutually compensates the oscillations. For simple enough potentials (such as barriers and wells) these functions can be obtained analytically. Once both sets of functions are obtained, the propagation follows a scheme much like the one pointed out by equation (23):

$$\Psi(x,t) = \sum_k c_k^L\,\mathrm{e}^{-\mathrm{i}E_k t}\varphi_k^L(x) + \sum_k c_k^R\,\mathrm{e}^{-\mathrm{i}E_k t}\varphi_k^R(x). \tag{27}$$

The projection coefficients c_k must account for the fact that this basis carries a degeneration of two eigenstates for every energy eigenvalue:

$$|c_k|^2 = \left|c_k^L\right|^2 + \left|c_k^R\right|^2. \tag{28}$$

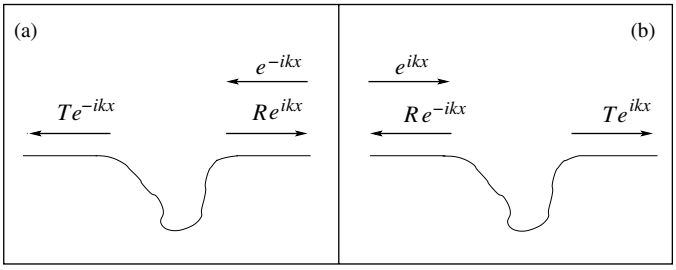

Figure 8. Basis set of outgoing eigenfunctions. (a) Waves φ_k^L outgoing to the left. (b) Waves φ_k^R outgoing to the right.

The outgoing boundary condition basis set was employed for the calculation of the spectral decomposition of a wavepacket moving in a free-potential region. We generate a basis of $N = 1500$ wavefunctions for each boundary condition, covering an energy region up to $E_N = 30$ au, where each eigenfunction φ_i has a wavenumber $k_i = i\Delta k$ with $\Delta k = \frac{\sqrt{2E_N}}{N} = 0.00516$ au, and the corresponding eigenvalue $E_i = \frac{k_i^2}{2}$. The results of the projection coefficients c_k as a function of the energy E_k for the same Gaussian wavepackets analysed in this section are displayed as the solid smooth curves in figures 6(b) and 7(b). Within the range covered in these figures (from 0 to 3 au), there are 474 eigenvalues. Therefore, it is not possible to mark the positions of the individual points along the smooth curves.

As shown in the figures, the use of the new basis set $\left\{\varphi_k^L, \varphi_k^R\right\}$ fully eliminates the spurious oscillations appearing in the projection to the stationary basis functions.

4. Practical application

As an example, in the present section we will show how the problems raised in the previous section are manifested in a real physical example. The case analysed here is the electron emission from metal surfaces induced by grazing incidence of ultrashort laser pulses. This is a widely developed area of current research, from both the theoretical and the experimental point of view.

When a laser pulse impinges at grazing incidence on a metal surface, an electron of the valence band of the solid can be ejected to the vacuum zone, ending in a final continuum state. The frame of reference is placed at the position of the crystal border, with the $\hat{z}$ axis in the direction perpendicular to the surface, aiming towards the vacuum region.

We consider a laser pulse associated with a linearly polarized electric field $F(t)$. According to the grazing incidence condition, the field $F(t)$ is oriented perpendicular to the surface, along the $\hat{z}$ axis. The temporal profile of the pulse is defined as

$$F(t) = F_0 \sin(\omega t + \varphi) \sin^2\left(\frac{\pi}{\tau} t\right), \tag{29}$$

for $0 < t < \tau$, and 0 elsewhere, where F_0 is the maximum field strength, ω is the carrier frequency, $\varphi = -\frac{\omega\tau}{2} + \frac{\pi}{2}$ represents the carrier-envelope phase and τ determines the duration of the pulse. In our simulation, we will use the parameters $F_0 = 0.5$, $\omega = 0.8$ and $\tau = 47.12$ au, producing the laser pulse displayed in figure 9.

In a previous work [17], we studied the electron emission coming from the valence band of Al(1 1 1) surfaces due to the grazing incidence of this type of ultrashort laser pulse. We solved there the corresponding time-dependent Schrödinger equation. In those calculations,

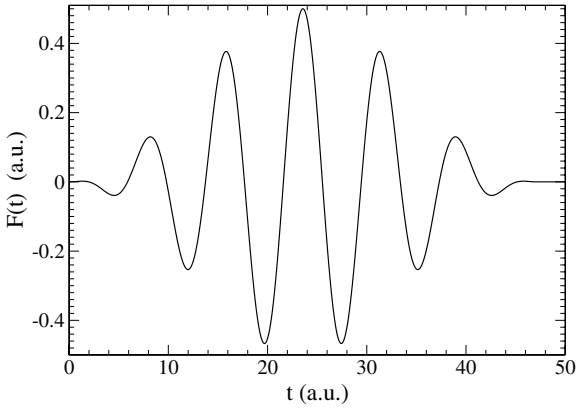

Figure 9. Temporal profile of the laser pulse (equation (29)), for $F_0 = 0.5$, $\omega = 0.8$ and $\tau = 47.12$ au.

the final emission is calculated by adding the contributions from any of the initial electronic states of the metal surface. For Al(1 1 1) we used about a hundred initial states, and found in some of our results quite a wide spread in the electron emission spectra. The oscillations in the final spectra may be a consequence of such a sum of many different transitions, and may also be associated with the use of a discrete grid. In the present case, we will focus only on a single transition, in order to ensure that only one kind of problem is isolated.

To describe the metal surface, we use the jellium model, in which the potential is represented by a square well potential of strength V_s:

$$V_s = E_F + E_W, \tag{30}$$

where E_F is the Fermi energy and E_W is the work function. This potential produces bound states very close to a more sophisticated parametric potential [18]. In order to obtain only one bound state, we will not use here the jellium potential parameters corresponding to Al(111) that produces 108 bounded levels. We have introduced a model jellium potential having a depth $V_s = 0.5$ au, and a width $L = 1.5$ au. Such a potential has a single bound state with an energy $E_b = -0.31$ au.

Since the Hamiltonian is time dependent, the propagation (23) can no longer be used. Therefore, we calculate the electron emission differential probability from the initial state i to any of the final continuum states k,

$$\frac{\partial P_{ik}}{\partial E_k} = \frac{|c_{ik}|^2}{\Delta E_k}, \tag{31}$$

where

$$c_{ik} = \langle \psi_i(x,t) | \varphi_k(x) \rangle \tag{32}$$

are the projection coefficients of the propagated wavefunction $\psi_i(x,t)$ towards the Hamiltonian eigenvector basis $\varphi_k(x)$, and the factor ΔE_k accounts for the density of states in such a way that

$$\int_0^\infty \frac{\partial P_{ik}}{\partial E_k} \, \mathrm{d}E_k = 1. \tag{33}$$

The propagated function is calculated, in turn, by

$$\psi_i(x,t) = \mathrm{e}^{-\mathrm{i}\hat{H}t} \psi_i(x,0) \tag{34}$$

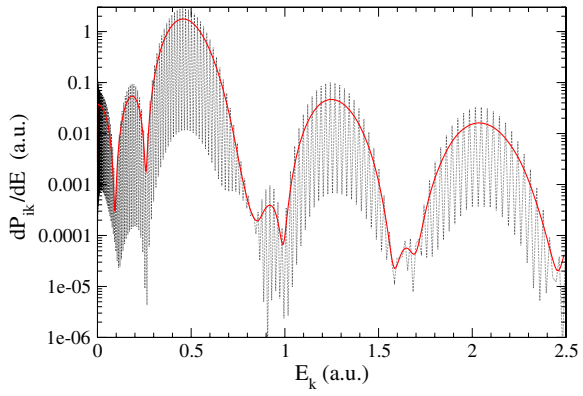

Figure 10. Differential probability of electron emission for the previous ultrashort laser pulse interacting with a (model) metal surface, as a function of the electron energy. Dotted lines: projection to stationary eigenvalues. Full curve: projection to left and right outgoing waves.

where $\psi_i(x,0)$ represents the wavefunction for the initial bound state i of the jellium potential (30). We must stress that in our calculations, the Hamiltonian eigenfunctions are not calculated from diagonalization. Therefore, equation (31) has been replaced by

$$\frac{\partial P_{ik}}{\partial E_k} = \frac{\left|c_{ik}^L\right|^2 + \left|c_{ik}^R\right|^2}{\Delta E_k}, \tag{35}$$

where

$$c_{ik}^P = \left\langle \psi_i(x,t) \middle| \varphi_k^P(x) \right\rangle \tag{36}$$

and $\varphi_k^P(x)$ represents the Hamiltonian eigenvector with outgoing boundary conditions to the left ($P = L$) or to the right ($P = R$).

The energy distribution spectrum of the emitted electrons ionized from the metal surface consists, in general, of a series of peaks separated by an energy $\Delta_E = \hbar\omega$. Each peak is related to the different order of multiphoton ionization [19]. The energy width of the peaks is inversely proportional to the duration time τ of the laser pulse, and eventually, for an infinitely long pulse, any peak will approach a Delta function. Since the laser pulse is very short, the envelope of the pulse may produce additional series of oscillations. The number of such oscillations occurring between the principal peaks corresponds to the ratio between the period $T = \frac{2\pi}{\omega}$ and the duration of the pulse τ.

In our model calculation, the laser pulse with $\omega = 0.8$ au, the first main peak appears at $E_k \approx 0.8 - 0.3 = 0.5$ au, the two-photon ionization peak appears at $E_k \approx 0.5 + 0.8 = 1.3$ au, etc. As shown in figure 10, the main peaks are too wide to allow the presence of the secondary peaks, so only a very few of them are notable in the spectrum.

The striking feature of figure 10 is the presence of huge oscillations, some of them of about three orders of magnitude. As explained above, the oscillations are a consequence of projecting the propagated wavefunction (which is mainly an even function), with successively odd and even stationary eigenfunctions. Utilizing the procedure proposed previously, we generated a new Hamiltonian eigenvalues basis set, having left and right outgoing boundary conditions. Using that basis set, we obtained the full smooth curve shown in the same figure, which eliminates completely all the spurious oscillations.

5. Conclusions

In spite of the simplicity and availability of computational codes suitable to perform numerical simulations of dynamical evolution of quantum systems, we have called attention here to some problems that may appear even in the simplest examples.

In section 2 we have shown a common issue in the numerical evolution of the Schrödinger equation at high energies: the space discretization determines an upper limit in the representable momenta. In order to solve this problem, the numerical grid must be adjusted, so as to include higher energies needed for an accurate description of the wavepacket.

In section 3 we have presented a much more elusive problem, predominantly occurring at low energies, where the projection on the Hamiltonian eigenvectors shows oscillations. These oscillations are produced by the parity of the stationary eigenfunctions. This problem cannot be solved by refining the numerical mesh. In section 3, we have presented the directions to construct a suitable basis, consisting of outgoing wavefunctions. As seen in the simple example of the evolution of a wavepacket in a free potential, the projection on this basis lacks a definite parity, and presents a smooth spectrum.

Finally, in section 4 we have shown a practical application of the issues raised in the present work. We have analysed there the electron emission from metal surfaces induced by grazing incidence of ultrashort laser pulses. The calculations presented in a previous work [17] were contaminated by a huge number of spurious oscillations. With the techniques presented here, we have shown that they may disappear, producing smooth ionization spectra.

Acknowledgments

We would like to acknowledge Drs Diego Arbó and Jorge Miraglia for several fruitful discussions. This work was supported by UBACyT X471 of Universidad de Buenos Aires.

References

[1] Griffiths D J 1995 *Introduction to Quantum Mechanics* (Upper Saddle River, NJ: Prentice-Hall)
[2] Goldberg A, Schey H M and Schwartz J L 1967 *Am. J. Phys.* **35** 177
[3] Chen R L W 1982 *Am. J. Phys.* **50** 902
[4] Maestri J J V, Landau R H and Páez M J 2000 *Am. J. Phys.* **68** 1113
[5] García A L 2000 *Numerical Methods for Physics* (Upper Saddle River, NJ: Prentice-Hall)
[6] Thaller B 2002 *Visual Quantum Mechanics* (New York: Springer)
[7] Landau R H, Paez M J and Bordeinau C C 2007 *Computational Physics, Problem Solving with Computers* 2nd edn (Berlin: Wiley-VCH)
[8] Landau R H 2008 *Am. J. Phys.* **76** 296
[9] Oppenheim A V, Schafer R W and Buck J R 1999 *Discrete-Time Signal Processing* 2nd edn (Englewood Cliffs, NJ: Prentice-Hall)
[10] van Dijk W and Toyama F M 2007 *Phys. Rev.* E **75** 036707
[11] Shao H and Wang Z 2009 *Phys. Rev.* E **79** 056705
[12] Sakurai J J 1994 *Modern Quantum Mechanics* revised edn (New York: Addison-Wesley) chapter II
[13] Cohen-Tannoudji C, Diu B and Laloë F 2006 *Quantum Mechanics* 2nd edn (New York: Wiley Interscience) chapter III–D.2
[14] '*First steps in quantum dynamics*', http://www.df.uba.ar/users/dmitnik/computation/dinamica/dinamica.html and '*Coherent states*', http://www.df.uba.ar/users/dmitnik/computation/coherentes/coherentes.html. Computational exercises for the undergraduate course of Modern Physics, Departamento de Física, Universidad de Buenos Aires, Argentina
[15] Schiff L I 1968 *Quantum Mechanics* 3rd edn (London: McGraw-Hill) pp 42–3
[16] Carjan N, Rizea M and Strottman D 2005 *Comput. Phys. Commun.* **173** 41
[17] Faraggi M N, Gravielle M S and Mitnik D M 2007 *Phys. Rev.* A **76** 012903
[18] Chulkov E V, Silkin V M and Echenique P M 1999 *Surf. Sci.* **437** 330
[19] Faisal F H M 1987 *Theory of Multiphoton Processes* (New York: Plenum)